Journal of Plant Physiology 168 (2011) 549–557

Contents lists available at ScienceDirect

Journal of Plant Physiology

journal homepage: www.elsevier.de/jplph

Spatial organization of the vindoline biosynthetic pathway in *Catharanthus roseus*

Grégory Guirimand[a,1], Anthony Guihur[a,1], Pierre Poutrain[a], François Héricourt[b], Samira Mahroug[c], Benoit St-Pierre[a], Vincent Burlat[a,2], Vincent Courdavault[a,*]

[a] *Université François Rabelais de Tours, EA 2106 "Biomolécules et Biotechnologies Végétales", IFR 135 "Imagerie fonctionnelle" 37200 Tours, France*
[b] *Université d'Orléans, EA1207 Laboratoire de Biologie des Ligneux et Grandes Cultures, and INRA, USC2030, Arbres et Réponses aux Contraintes Hydrique et Environnementales (ARCHE), 45067 Orléans, France*
[c] *Laboratoire Biodiversité Végétale, Conservation et Valorisation - Faculté des Sciences - Université Djillali Liabés - Sidi Bel Abbes 22000, Algerie*

ARTICLE INFO

Article history:
Received 14 April 2010
Received in revised form 25 August 2010
Accepted 25 August 2010

Keywords:
Alkaloid
Bimolecular fluorescence complementation
Catharanthus roseus
O-methyltransferase
Vindoline

ABSTRACT

Vindoline constitutes the main terpenoid indole alkaloid accumulated in leaves of *Catharanthus roseus*, and four genes involved in its biosynthesis have been identified. However, the spatial organization of the tabersonine-to-vindoline biosynthetic pathway is still incomplete. To pursue the characterization of this six-step conversion, we illustrated, with *in situ* hybridization, that the transcripts of the second biosynthetic enzyme, 16-hydroxytabersonine 16-*O*-methyltransferase (16OMT), are specifically localized to the aerial organ epidermis. At the subcellular level, by combining GFP imaging, bimolecular fluorescence complementation assays and yeast two-hybrid analysis, we established that the first biosynthetic enzyme, tabersonine 16-hydroxylase (T16H), is anchored to the ER as a monomer via a putative N-terminal helix that we cloned using a PCR approach. We also showed that 16OMT homodimerizes in the cytoplasm, allowing its exclusion from the nucleus and thus facilitating the uptake of T16H conversion product, although no T16H/16OMT interactions occur. Moreover, the two last biosynthetic enzymes, desacetoxyvindoline-4-hydroxylase (D4H) and deacetylvindoline-4-*O*-acetyltransferase (DAT), were shown to operate as monomers that reside in the nucleocytoplasmic compartment following passive diffusion to the nucleus allowed by the protein size. No D4H/DAT interactions were detected, suggesting the absence of metabolic channeling in the vindoline biosynthetic pathway. Finally, these results highlight the importance of the inter- and intracellular translocations of intermediates during the vindoline biosynthesis and their potential regulatory role.

Introduction

Terpenoid indole alkaloids (TIA) form an important group of secondary metabolites synthesized in the Apocynaceae. Among the numerous TIA, vinblastine and vincristine produced in the Madagascar periwinkle (*Catharanthus roseus*) are of particular importance because of their anticancer properties and their wide use in chemotherapy treatment. These two dimeric TIA are synthesized in aerial organs of *C. roseus* through the condensation of two monomeric TIA, catharanthine and vindoline. Currently, the dimeric TIA and their derivates used in anticancer treatment are hemisynthesized from vindoline and catharanthine extracted from *C. roseus* leaves. Due to the low abundance of these two TIA, numerous studies have been engaged over the past 20 years to elucidate their biosynthetic pathway. The biosynthesis of vindoline results from a six-enzymatic reaction mediated conversion of tabersonine (Fig. 1). The first step of this biosynthetic pathway involves the hydroxylation of tabersonine catalyzed by tabersonine 16-hydroxylase (T16H; CYP71D12; EC 1.14.13.73), a cytochrome P450-dependent enzyme (St-Pierre and De Luca, 1995; Schröder et al., 1999). The resulting 16-hydroxytabersonine is next *O*-methylated by 16-hydroxytabersonine 16-*O*-methyltransferase (16OMT; EC 2.1.1.94), which has been recently cloned (Levac et al., 2008). The third reaction is catalyzed by an unidentified hydratase that performs the hydratation of the 2,3 double bond, while the subsequent step of N-methylation involves a partially characterized *N*-methyltransferase (NMT) producing desacetoxyvindoline (De Luca et al., 1987). The penultimate step catalyzed by desacetoxyvindoline-4-hydroxylase (D4H; EC 1.14.11.20) produces

Abbreviations: 16OMT, 16-hydroxytabersonine 16-*O*-methyltransferase; BiFC, bimolecular fluorescence complementation; D4H, desacetoxyvindoline-4-hydroxylase; DAT, deacetylvindoline-4-*O*-acetyltransferase; TIA, terpenoid indole alkaloids; LCM, laser-capture microdissection; SLS, secologanin synthase; T16H, tabersonine 16-hydroxylase.

* Corresponding author at: Université François-Rabelais de Tours, EA 2106 "Biomolécules et Biotechnologies Végétales", UFR des Sciences et Techniques, 37200 Tours, France. Tel.: +33 247 36 69 88; fax: +33 247 27 66 60.
E-mail address: vincent.courdavault@univ-tours.fr (V. Courdavault).
[1] Both authors have contributed equally to this work.
[2] Present address: Université de Toulouse, UPS, UMR 5546, Surfaces Cellulaires et Signalisation chez les Végétaux, BP 42617, F-31326, Castanet-Tolosan, France.

0176-1617/$ – see front matter © 2010 Elsevier GmbH. All rights reserved.
doi:10.1016/j.jplph.2010.08.018

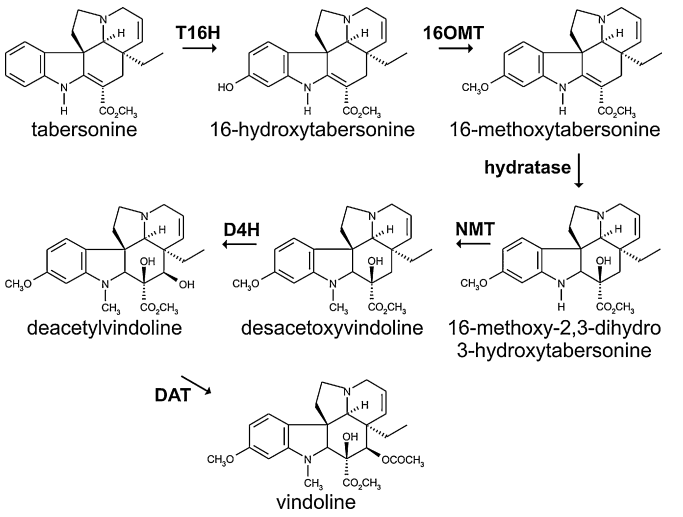

Fig. 1. The biosynthesis of vindoline from tabersonine. Tabersonine is converted into vindoline through a series of 6 reactions catalyzed by tabersonine 16-hydroxylase (T16H), 16-hydoxytabersonine-16-*O*-methyltransferase (16OMT), uncharacterized hydratase and *N*-methyltransferase (NMT), desacetoxyvindoline-4-hydroxylase (D4H) and deacetylvindoline-4-*O*-acetyltransferase (DAT).

deacetylvindoline (De Carolis et al., 1990; Vazquez-Flota et al., 1997). The last step is the acetylation of deacetylvindoline by deacetylvindoline-4-*O*-acetyltransferase (DAT; EC 2.3.1.107) to form vindoline (De Luca et al., 1985; St-Pierre et al., 1998). *In planta*, the vindoline biosynthesis appears as a tightly regulated mechanism affected by developmental or differentiation processes and by the compartmentation of the vindoline biosynthetic enzymes (Westekemper et al., 1980; St-Pierre et al., 1999). The importance of inter- and intracellular translocations of intermediates resulting from the compartmentation of enzymes has also emerged as a central regulatory mechanism in distinct natural product biosynthesis (Kutchan, 2005). While several studies have been engaged to characterize the cellular and sub-cellular organization of the vindoline biosynthetic pathway (reviewed in Guirimand et al., 2010a), the elucidation of the compartmentation is still incomplete. For instance, in aerial organs, the D4H and DAT enzymatic steps have been localized to laticifers/idioblast specialized cells while epidermal cells harbor the reactions located between the final step of the biosynthesis of the TIA monoterpenoid precursor catalyzed by secologanin synthase (SLS; CYP72A1; EC 1.3.3.9) and 16OMT including T16H (St-Pierre et al., 1999; Irmler et al., 2000; Murata and De Luca, 2005; Levac et al., 2008; Murata et al., 2008; Roepke et al., 2010). However, the situation is less clear for these two enzymes because their transcripts were solely detected by RT-PCR approaches that do not allow a complete overview of the mRNA distribution, as observed, for example using *in situ* hybridization for D4H and DAT. At the subcellular level, the distribution of 16OMT and D4H has not been investigated and the sole data available for T16H and DAT were obtained from density gradient analysis (De Luca and Cutler, 1987; St-Pierre and De Luca, 1995). This approach leads to artefactual results, particularly for TIA biosynthetic enzymes, as demonstrated previously (Guirimand et al., 2009, 2010b). In addition, there have been no reports on the subcellular organization of these enzymes, while the formation of metabolons has been widely described in plant secondary metabolism (Jørgensen et al., 2005). This prompted us to evaluate the cellular and sub-cellular localization of the vindoline biosynthetic enzymes in *C. roseus* cells using RNA *in situ* hybridization and GFP imaging, and to study possible interactions using Bimolecular Fluorescence Complementation (BiFC) and yeast two-hybrid assays. These new results allow us to better characterize the architecture of the vindoline pathway and to identify possible steps of biosynthetic intermediate translocation.

Materials and methods

Amplification of the 5′-end of T16H

The 5′-end of T16H cDNA was amplified via an asymmetric PCR performed on a λZAPII-oriented *Catharanthus roseus* cDNA library using the M13 reverse universal primer and the specific forward T16H-2 primer (see Supplementary Table 1 for details on all primers used in this study). The amplified cDNA was cloned in pSC-A amp/kan (Stratagene) and sequenced.

Biolistic-mediated transient transformation of C. roseus suspension cells and GFP imaging

Transient transformation of *C. roseus* cells by particle bombardment and GFP imaging were performed following the procedures described by Guirimand et al. (2009, 2010b). Briefly, cells plated onto solid culture medium were bombarded, using the Bio-Rad PDS1000/He system, with DNA coated gold particles (1 μm) and a 1100 psi rupture disk at a stopping-screen-to-target distance of 6 cm. Bombarded cells were cultivated 15 h prior studying protein sub-cellular localization using an Olympus BX-51 epifluorescence microscope equipped with an Olympus DP-71 digital camera.

YFP-fused enzyme expression vectors

To construct the T16H–YFP expression vector, the full length T16H ORF (GenBank FJ647194) was amplified by PCR using primers T16H-BglII and T16H-SpeI. For thT16H–YFP expression vector, the coding sequence of the putative transmembrane helix (first 24 residues of T16H including 3 residues downstream of the transmembrane helix) was amplified by combining primers T16H-BglII and pep-T16H-SpeI. The ΔthT16H–YFP expression vector expressing a transmembrane helix deleted version of T16H was constructed following amplification of the coding sequence of the remaining part of the protein (residues T22-A506) using primers T16H-del and T16H-SpeI allowing the addition of an initiation codon prior to residue 22 of the deleted version of T16H. These cDNAs were sequenced and cloned into the *Bgl*II and *Spe*I restriction sites of pSCA-cassette YFPi (Guirimand et al., 2009) in frame with the 5′-extremity of the coding sequence of YFP driven by the CaMV35S promoter to express the fusion protein. The 16OMT–YFP and YFP–16OMT expression vectors were constructed following amplification of the coding sequence of 16OMT (GenBank EF444544) with primers 16OMT-GFPfor and 16OMT-GFPrev allowing the addition of *Spe*I restriction sites at both the 5′ and 3′ extremities of the amplified sequence. After sequencing, the 16OMT cDNA was cloned either into the *Spe*I or in the compatible *Nhe*I restriction site of pSCA-cassette YFPi to express 16OMT–YFP or YFP–16OMT, respectively. A similar approach was used to construct the plasmids expressing D4H–YFP, YFP–D4H, DAT–YFP and YFP–DAT except that *Nhe*I restriction sites were added at the extremity of the DAT coding sequence.

Bimolecular fluorescence complementation (BiFC) assays

BiFC assays were carried out using the pSPYNE(R)173, pSPYCE(MR), pSPYNE173 and pSPYCE(M) plasmids that allow the *Spe*I-cloning at the 5′ or 3′ ends of the coding sequence of the N-terminal (YFP^N, residues 1–173) and C-terminal (YFP^C, residues 156–239) fragments of YFP (Waadt et al., 2008). cDNAs were amplified as described in the previous section except for T16H, for which

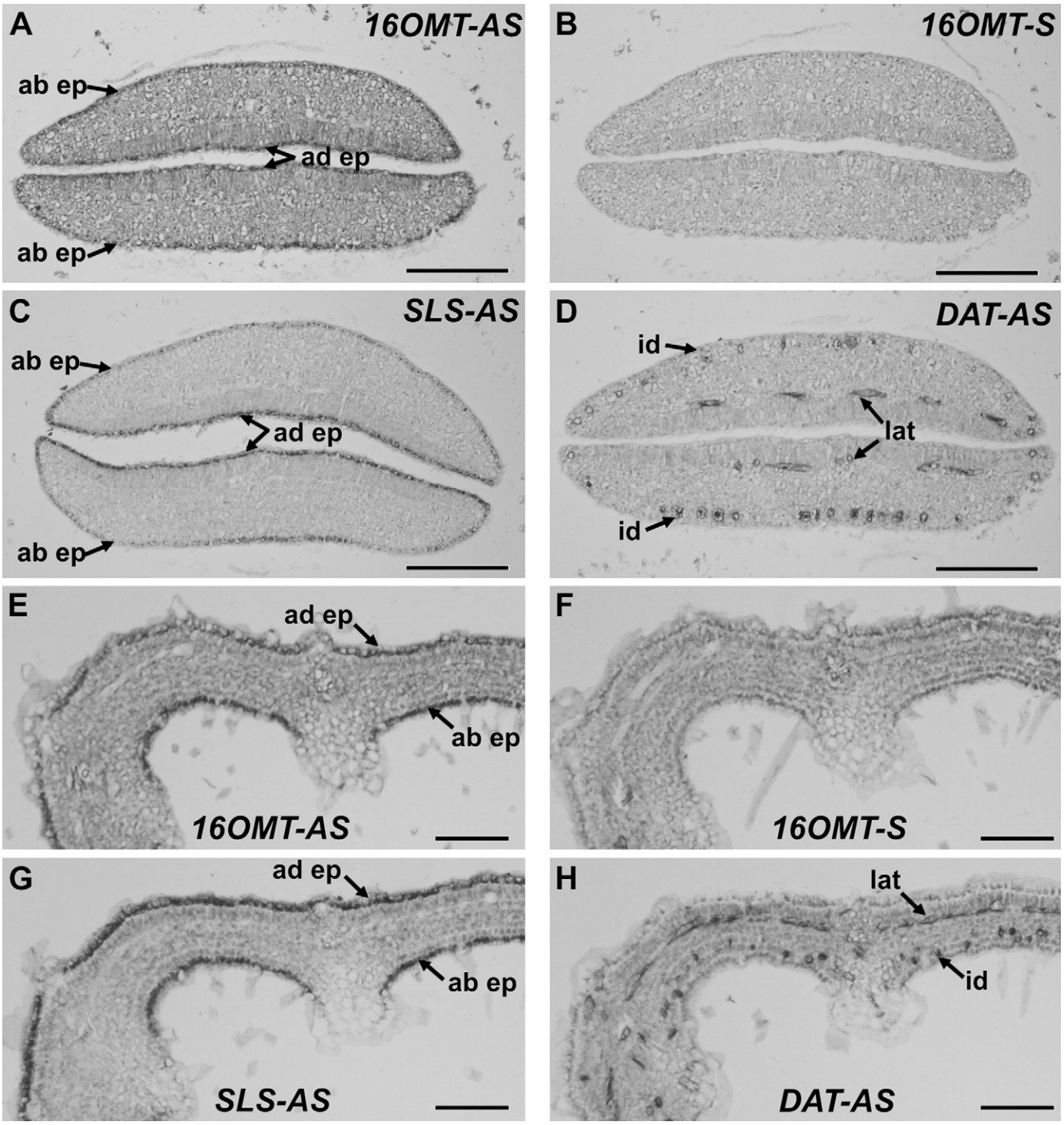

Fig. 2. 16OMT transcripts are specifically located in the epidermis of *C. roseus* aerial organs. Serial sections of cotyledons (A–D) and young developing leaves (E–H) were hybridized either with 16OMT-antisense (AS) probes (A and E), with 16OMT-sense (S) probes (B and F) used as a negative control or with SLS-AS (C and G) probes and DAT-AS probes (D and H) used as positive controls. ab, abaxial; ad, adaxial; id, idioblast; lat, laticifer; ep, epidermis. Bar: 100 μm.

we used the combination of primers T16Hfor-SpeI and T16H-SpeI (Supplementary Table 1).

Organelle markers and cell co-transformation

ER CFP marker (CD3-954) was obtained from the ABRC (http://www.arabidopsis.org). The nucleocytoplasm CFP marker was generated following amplification of the CFP coding sequence using primers CFPfor2 and CFP2rev-NheI and cloning into the *Bgl*II and *Nhe*I restriction sites of pSCA-cassette YFPi (Guirimand et al., 2009) to substitute the YFP coding sequence (Supplementary Fig. 1). For the nucleus CFP marker, the CFP coding sequence was cloned into the BglII and SpeI restriction sites of pCAMBIA 1305 (obtained from CambiaLabs at http://www.cambia.org; GenBank AF354045) to generate a CFP-GUS fusion protein. The nuclear localization sequence (NLS) of a *Xenopus* nucleoplasmin (NP_001081027) was next added at the N-terminal end of CFP-GUS following the annealing of primers NLS-nucleo for and NLS-nucleo rev and cloning of the

resulting sequence into the *Bgl*II and *Spe*I restriction sites of pCAMBIA 1305 CFP-GUS. Plasmid co-transformations were performed according to Guirimand et al. (2009) using 400 ng of each plasmid or 100 ng for BiFC assays.

Yeast two-hybrid

The yeast two-hybrid analysis was performed using a LexA DNA-binding domain-encoding bait vector (pBTM116 referred as pLex) and a Gal4 activation domain-encoding prey vector (pGADT7, Clontech). After amplification using each combination of 2yeast-primers (Supplementary Table 1), a *BamH*I cloning was performed in both vectors. Co-transformant yeasts (strain L40Δ) were selected onto leucine–trytophan lacking medium (−LW) for 4 days at 30 °C and then streaked onto leucine–trytophan–histidine lacking medium (−LWH) and grown for 4 days at 30 °C. Due to weak autoactivation of hybrid proteins, the −LWH medium was supplemented with 5 mM 3-amino-1,2,4-triazole (3AT). X-Gal assays were performed according to the overlay method derived from Fromont-Racine et al. (1997).

In situ RNA hybridization of C. roseus leaves and cotyledons

Full-length 16OMT cDNA cloned in pSC-A amp/kan were used for the synthesis of sense and anti-sense RNA probes as previously described (Mahroug et al., 2006). For SLS and DAT, previously described plasmids were used for the riboprobe transcription (St-Pierre et al., 1999; Irmler et al., 2000). Paraffin-embedded serial longitudinal sections of young developing and mature leaves and transversal sections of emerging cotyledons were hybridized with digoxigenin-labeled transcripts and localized with anti-digoxigenin–alkaline phosphatase conjugates according to Mahroug et al. (2006).

Results

The 16OMT transcripts show a specific epidermal localization

To complete the RT-PCR analysis of the mRNA distribution of the first enzymes of the vindoline biosynthetic pathway (Levac et al., 2008), we performed an *in situ* RNA hybridization of the 16OMT transcripts in cotyledons of *Catharanthus roseus* young seedlings and young developing and mature leaves (Fig. 2). In both types of young aerial organs, the 16OMT mRNA were specifically detected in adaxial and abaxial epidermis with the antisense probe, while no signal was revealed using the sense probe (Fig. 2A, B, E and F). The other cell types did not express the 16OMT transcripts, while as controls, the SLS and DAT transcripts where detected in adaxial/abaxial epidermis and laticifers/idioblasts, respectively (Fig. 2C, D, G and H). No signal was detected in mature leaves (data not shown), a result in agreement with the down-regulation of TIA biosynthetic gene expression observed in older organs (St-Pierre et al., 1998, 1999).

T16H is an endoplasmic reticulum anchored enzyme

The subcellular localization of the four characterized enzymes of the vindoline biosynthetic pathway (T16H, 16OMT, D4H and DAT) was studied using a combined approach of biolistic-mediated transient transformation of *C. roseus* cells and GFP imaging. In a first step, due to the lack of several residues at the N-terminal end of T16H (AJ238612; Schröder et al., 1999), the 5′-end of the corresponding cDNA was cloned by PCR. The amplified cDNA harbors 50 additional base pairs, upstream of the original sequence and encompasses an 11-residue ORF initiated by an ATG codon in frame with the T16H coding sequence (Fig. 3). The identification

```
1   GGCATGAGCATTTTCACTCATGGAATTCTATTATTTTCTCTAC
1         *               M  E  F  Y  Y  F  L  Y

43  TTGGCCTTCCTTCTTTTCTGCTTCATTTTATCAAAAACCACAA
9    L  A  F  L  L  F  C  F  I  L  S  K  T  T
```

Fig. 3. Nucleotide and deduced residue sequences of the T16H 5′-end. The sequence cloned in this work is designated using normal letters whereas the previously known sequence appears in italics. (*) designates a stop codon.

of an upstream termination signal (TGA) in frame with the putative initiation codon definitively validated this initiation codon. Based on this result, the T16H full-length ORF was amplified (GenBank FJ647194) allowing the identification of a putative N-terminal 18-residue transmembrane helix (residue Y4-T21; Supplementary Fig. 2 and Table 2). To maintain the accessibility of the helix, the T16H full-length ORF was cloned in frame with the 5′-extremity of the YFP coding sequence to generate a T16H–YFP fusion protein. In transiently transformed cells, the fluorescence signal of the fusion protein appeared as a network structure branching all across the cell and surrounding the nucleus (Fig. 4A–D) and perfectly co-localized with the "ER"-CFP marker (Fig. 4E–H). This ER localization was dependent on the presence of the putative transmembrane helix, as revealed by the ER localization of the YFP-fused protein bearing solely the first 24 residues of T16H (thT16H; residues M1-K24) and by the absence of ER targeting for the deleted protein (ΔthT16H; residues T22-A506), as shown in Fig. 4I–P.

16OMT is organized as homodimers in the cytosol

To clearly identify the subcellular localization of 16OMT, a GFP imaging analysis was also performed. As an initial step, a predictive study of localization was performed using bioinformatic software. This yielded contradictory results, including a possible targeting to peroxisome due to a peroxisomal targeting sequence (SKL, residue S178-L180) or to plastid stroma or thylakoid membrane, although no plastid targeting sequence could be identified (Supplementary Table 2). To avoid a possible masking of such sequences that could lead to artefactual results, the 16OMT full length ORF was cloned either at the 5′-end or at the 3′-end of the YFP coding sequence to express 16OMT–YFP and YFP–16OMT fusion proteins in *C. roseus* cells. For both constructs, the fusion proteins displayed a fluorescence signal located in the nucleocytoplasm, as revealed by the perfect merging with the signal emitted by the CFP nucleocytoplasmic marker (Fig. 5A–H). To gain insight into the conformational organization of 16OMT *in vivo*, BiFC assays were also conducted. Following the cloning of the 16OMT coding sequence in the BiFC vectors, the four plasmid combinations were transiently expressed in *C. roseus* cells. Co-transformations of plasmids expressing the 16OMT fused to the same extremity of the split-YFP fragments (*e.g.* 16OMT–YFP^N/16OMT–YFP^C and YFP^N-16OMT/YFP^C-16OMT) specifically allow the formation of a BiFC complex visualized as a fluorescent signal within the cells, suggesting that 16OMT is able to homodimerize (Fig. 6A–H, Supplementary Fig. 3). In contrast to the nucleocytoplasmic localization of 16OMT–YFP and YFP–16OMT (Fig. 5), the 16OMT–BiFC complexes displayed an exclusive cytosolic localization, as revealed by their exclusion from the nucleus when compared to the nucleocytoplasmic CFP marker (Fig. 6I–L) and by the perfect merging with the cytoplasmic marker (CFP-GUS) (Fig. 6M–P). No fluorescence was detected when 16OMT was fused at the opposite orientations, either upstream or downstream of the split-YFP fragments, suggesting that the interactions of 16OMT are dependent on the fusion orientation. In addition, 16OMT self-interaction was monitored by yeast two-hybrid experiments. Co-transformation of yeast with the prey construct carrying

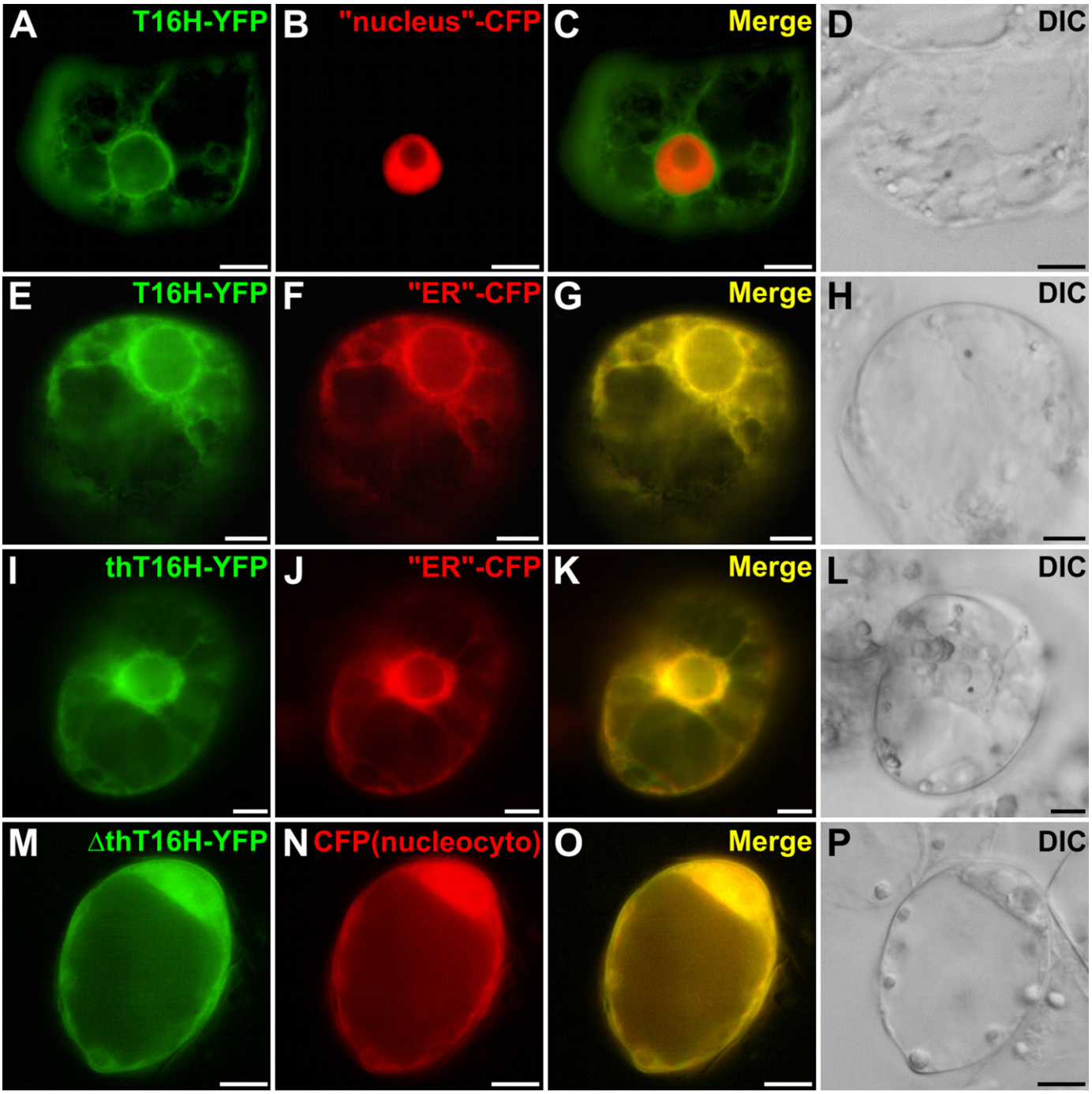

Fig. 4. Subcellular localization of T16H and functional characterization of the N-terminal transmembrane helix in *C. roseus* cells. Cells were transiently transformed with T16H–YFP (A–H), thT16H–YFP (I–L) or ΔthT16H–YFP (M–P) expressing vectors in combination with different markers as mentioned on the images of the first two columns. Co-localization of the two fluorescence signals appeared on the merged image. The morphology is observed with differential interference contrast (DIC). th, transmembrane helix; Δth, absence of the th; nucleocyto, nucleocytoplasm. Bar: 10 μm.

the 16OMT/GAL4 activation domain (AD) fusion and the bait construct harboring the 16OMT/LexA DNA-binding domain (BD) fusion allows the recovery of yeast growth on selective medium and the acquirement of β-galactosidase activity indicating a strong protein–protein interaction (Table 1; Supplementary Fig. 4). No yeast growth was recovered when 16OMT/GAL4 AD or 16OMT/Lex BD were expressed with Lex BD and GAL4 AD alone or as with fusion with D4H and DAT, validating the self interaction of 16OMT. BiFC assays also revealed the absence of 16OMT–T16H and T16H–T16H interactions (data not shown).

Table 1
Analysis of 16OMT, D4H and DAT interaction using yeast two-hybrid assays. +++ and – symbolize strong and no interaction between the partners, respectively.

	pLex-OMT	pLex-D4H	pLex-DAT	pLex
pGAD-OMT	+++	–	–	–
pGAD-D4H	–	–	–	–
pGAD-DAT	–	–	–	–
pGAD	–	–	–	–

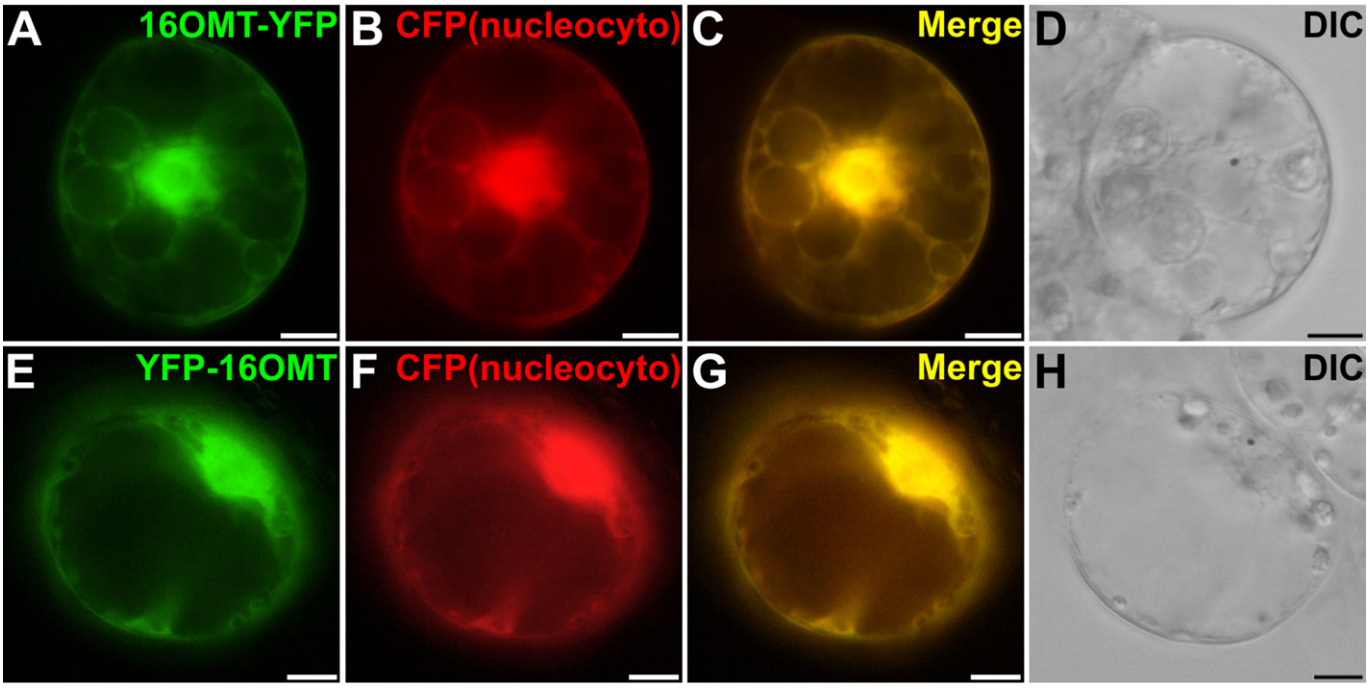

Fig. 5. Subcellular localization of 16OMT in *C. roseus* cells. Cells were transiently transformed with 16OMT–YFP (A–D) or YFP–16OMT (E–H) expressing vectors in combination with the nucleocytoplasmic (nucleocyto) CFP marker. Co-localization of the two fluorescence signals appeared on the merged image. The morphology is observed with differential interference contrast (DIC). Bar: 10 μm.

D4H and DAT are nucleocytoplasmic enzymes

The bioinformatic predictions of D4H and DAT subcellular localization also led to ambiguous and/or contradictory results. As an example, D4H has been predicted to be a membrane-anchored enzyme (plasma, ER, or thylakoid membrane), while no transmembrane helix could be identified. Moreover, a plastid/thylakoid-targeting of DAT was predicted, while no plastid targeting peptide was detected within the sequence (Supplementary Table 2). As a consequence, both D4H and DAT were fused either to the N-terminal or C-terminal end of GFP and transiently expressed in *C. roseus* cells. Irrespective to the fusion orientation, both D4H and DAT were localized to the cytoplasm and the nucleus, as highlighted by the perfect overlapping of the fluorescence signal of the fusion proteins with the nucleocytoplasmic CFP marker (Fig. 7A–P). In addition, no D4H or DAT homodimerization and no D4H and DAT heterodimerization were detected by BiFC assays (data not shown) and/or by yeast two-hybrid experiments (Table 1, Supplementary Fig. 4) for any plasmid associations.

Discussion

Vindoline, which belongs to the TIA Aspidosperma family, is the main alkaloid accumulated in *C. roseus* leaves (Westekemper et al., 1980) and constitutes one of the two precursors of the highly valuable anticancer TIA, vinblastine and vincristine. Consequently, the cellular and subcellular organization of the vindoline biosynthetic pathway has been intensely studied since the first characterization of the DAT activity in *C. roseus* leaf extracts (De Luca et al., 1985). Although a wide range of analytical techniques has been used to perform such studies, including RNA *in situ* hybridization, immunolocalization, laser-capture microdissection (LCM)-assisted RT-PCR, epidermis-enriched EST or density gradient analysis, the organization of this biosynthetic pathway is still incompletely characterized. At the cellular level, it is now admitted that the two last steps catalyzed by D4H and DAT are located to laticifers and idioblats (St-Pierre et al., 1999; Murata et al., 2008). The T16H and 16OMT transcripts were detected mainly in epidermis by LCM assisted RT-PCR and by epidermis EST analysis (Murata and De Luca, 2005; Murata et al., 2008). However, such analytical techniques do not allow observation of the complete mRNA distribution within the leaves since they are restricted to the tissues used for RNA extraction. We therefore performed RNA *in situ* hybridizations to complete the RT-PCR analysis with particular focus on the 16OMT since it acts downstream of T16H. Our results confirmed that 16OMT transcripts are largely, if not exclusively, located in the young aerial organ epidermis (Fig. 2). This supports the fact that the metabolites transported from epidermis to laticifers/idioblasts are produced either by 16OMT, the unknown hydratase or NMT (Fig. 1). At the subcellular level, our combined approach of primary sequence analysis, GFP imaging and fusion/deletion experiments allowed us to show that T16H is localized to the ER as a monomer in agreement with the results of St-Pierre and De Luca (1995) (Fig. 4). This ER localization is dependent on the presence of a putative N-terminal transmembrane helix that has not been identified previously due to the incomplete cloning of the T16H cDNA. Such a helix could allow the anchoring of T16H to the ER, exposing the catalytic domain of the protein toward the cytosol in agreement with the membrane topology of cytochrome P450 (Schuler and Werck-Reichhart, 2003). Irrespective to the YFP orientation, we established that 16OMT displayed a nucleocytoplasmic localization (Fig. 5A–H). In addition, we also showed, using BiFC assays and yeast two-hybrid experiments, that 16OMT is organized as homodimers *in vivo* (Figs. 5A-H and 6A–P, Table 1). Such homodimerization seems to be a common feature of plant *O*-methyltransferases and has been reported for other enzymes, such as flavone OMT (Kornblatt et al., 2008). Interestingly, the 16OMT homodimers are localized in the cytoplasm with exclusion from the nucleus (Fig. 6A–P). This is likely to be due to the homodimer size (79.6 kDa and 106.6 kDa without and with YFP, respectively), which is larger than the size exclusion limit of the nuclear pores allowing passive diffusion (60 kDa; Weis, 2003). On the contrary, the fusion to a full-length YFP would

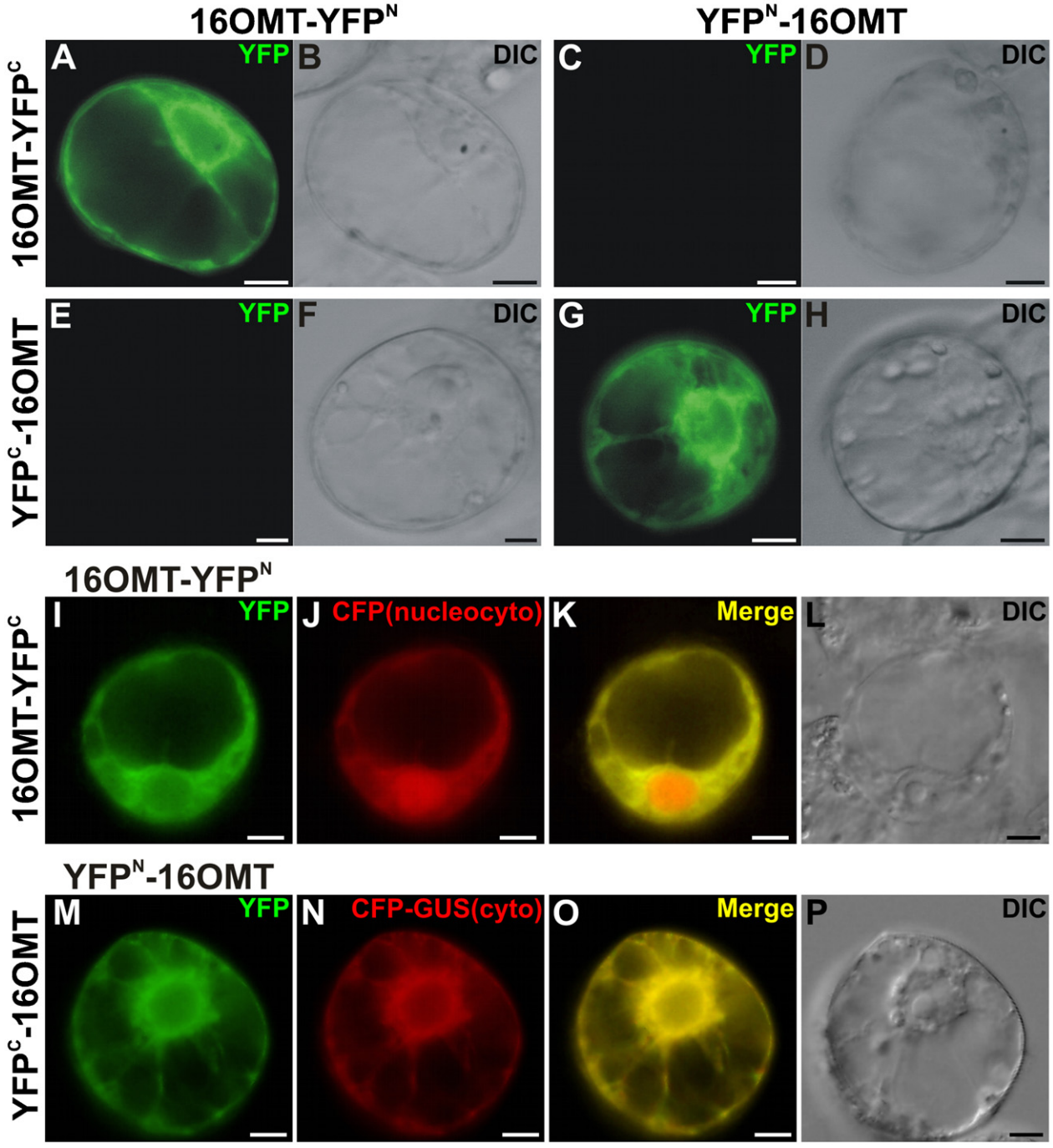

Fig. 6. Analysis of 16OMT homodimerization in *C. roseus* cells using BiFC assays. (A–H) Cells were co-transformed using a combination of plasmids as indicated on the top (fusion with the YFP^N fragment) and on the left (fusion with the YFP^C fragment). For the two combinations leading to BiFC complex reformation an additional co-transformation was performed with the CFP nucleocytoplasmic (I–L) or the CFP-GUS cytoplasmic (M–P) marker. The morphology is observed with differential interference contrast (DIC). Bar: 10 μm.

not allow 16OMT dimerization, probably due to problems of steric hindrance, causing the passive diffusion into the nucleus (Fig. 5). From a physiological point of view, it could be hypothesized that the cytosol sequestration of 16OMT would facilitate the uptake of the 16-hydroxytabersonine released in the cytosol by ER-anchored T16H. In addition, while numerous metabolons including P450 have been described in particular with OMT (Liu and Dixon, 2001), no interaction between T16H and 16OMT has been detected using BiFC assays, suggesting that no metabolic channeling occurs within the first steps of vindoline biosynthesis. On the contrary, the lack of interaction between T16H and D4H or DAT was expected due to the cellular compartmentation of these enzymes in epidermis and laticifers/idioblasts, respectively. While no data were available concerning D4H, we provided results arguing for a nucleocytoplasmic localization of both D4H and DAT (Fig. 7). This is partially in agreement with the results of De Luca and Cutler (1987), who described DAT as a cytosolic enzyme, and with the suggestion of De Carolis et al. (1990) about a D4H cytoplasmic localization. Such distribution in both the nucleus and the cytoplasm is probably due to a passive diffusion across nuclear pores since D4H and DAT are smaller than 50 kDa and no nuclear localization sequences were identified (Supplementary Table 2). In our experiments, the fusion with YFP

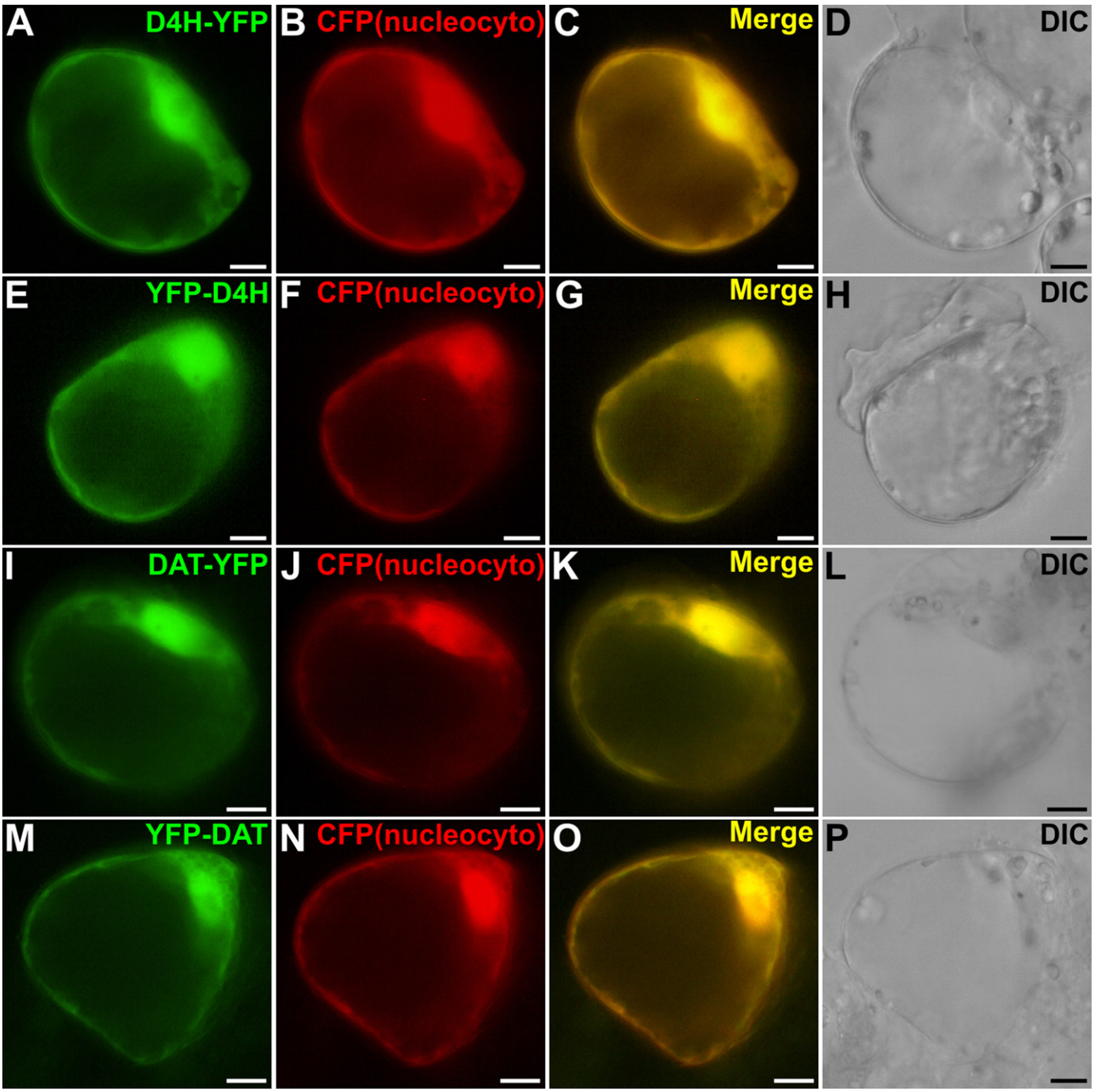

Fig. 7. Subcellular localization of D4H and DAT in *C. roseus* cells. Cells were transiently transformed with D4H–YFP (A–D), YFP–D4H (E–H), DAT–YFP (I–L) or YFP–DAT (M–P) expressing vectors in combination with the nucleocytoplasmic (nucleocyto) CFP marker. Co-localization of the two fluorescence signals appeared on the merged image. The morphology is observed with differential interference contrast (DIC). Bar: 10 μm.

increased the size of the proteins (about 75 kDa for both), but it has already been shown that proteins larger than 80 kDa could diffuse through nuclear pores depending on their nature (Wang and Brattain, 2007). In addition, the absence of homo- and heterodimerization would avoid the sequestration of D4H and DAT in the cytoplasm as observed for 16OMT (Table 1) and is in agreement with the protein size estimated during purification (De Luca et al., 1985; De Carolis et al., 1990). This nucleocytoplasmic localization has been recently described for other acyltransferases, such as anthocyanin/flavonol acyltransferase (Yu et al., 2008). The presence of TIA biosynthetic enzymes in the nucleus, such as D4H and DAT (this study) and strictosidine β-D-glucosidase (Guirimand et al., 2010b), as well as flavonoid biosynthetic enzymes including chalcone synthase and isomerase (Saslowsky et al., 2005) also suggests that an active secondary metabolism takes place in this compartment. In conclusion, based on our results and those from De Luca's group, it appears that the biosynthesis of vindoline from tabersonine sequentially takes place at least in two cell types including epidermis (T16H, 16OMT) and laticifers/idioblasts (D4H, DAT) and involves at least four subcellular compartments including ER (anchoring of T16H), cytosol (dimerized 16OMT, soluble D4H and DAT), plastids (NMT) and nucleus (passive diffusion of D4H and DAT) without apparent formation of metabolons between the four enzymes. The cartography of the almost fully characterized

vindoline biosynthetic pathway (an unknown hydratase remains to be characterized) suggests that the resulting inter- and intracellular exchanges could constitute regulatory mechanisms of TIA biosynthesis.

Acknowledgements

This research was financially supported by the Ministère de l'Enseignement Supérieur et de la Recherche and by a grant from the University of Tours. We acknowledge Prof. Jörg Kudla (Universität Münster) for the BiFC vectors.

Appendix A. Supplementary data

Supplementary data associated with this article can be found, in the online version, at doi:10.1016/j.jplph.2010.08.018.

References

De Carolis E, Chan F, Balsevich J, De Luca V. Isolation and characterization of a 2-oxoglutarate dependent dioxygenase involved in the second-to-last step in vindoline biosynthesis. Plant Physiol 1990;94:1323–9.

De Luca V, Balsevich J, Kurz WGW. Acetyl coenzyme A: deacetylvindoline *O*-acetyltransferase, a novel enzyme from *Catharanthus*. J Plant Physiol 1985;121:417–28.

De Luca V, Balsevich J, Tyler RT, Kurz WGW. Characterization of a novel N-methyltransferase (NMT) from *Catharanthus roseus* plants. Plant Cell Rep 1987;6:458–61.

De Luca V, Cutler AJ. Subcellular localization of enzymes involved in indole alkaloid biosynthesis in *Catharanthus roseus*. Plant Physiol 1987;85:1099–102.

Fromont-Racine M, Rain JC, Legrain P. Toward a functional analysis of the yeast genome through exhaustive two-hybrid screens. Nat Genet 1997;16:277–82.

Guirimand G, Burlat V, Oudin A, Lanoue A, St-Pierre B, Courdavault V. Optimization of the transient transformation of *Catharanthus roseus* cells by particle bombardment and its application to the subcellular localization of hydroxymethylbutenyl 4-diphosphate synthase and geraniol 10-hydroxylase. Plant Cell Rep 2009;28:1215–34.

Guirimand G, Courdavault V, St-Pierre B, Burlat V. Biosynthesis and regulation of alkaloids. In: Pua EC, Davey MR, editors. Plant developmental biology—biotechnological perspectives, vol. 2. GmbH Berlin Heidelberg: Springer-Verlag; 2010a. p. 139–60.

Guirimand G, Courdavault V, Lanoue A, Mahroug S, Guihur A, Blanc N, et al. Strictosidine activation in Apocynaceae: towards a "nuclear time bomb?". BMC Plant Biol 2010b;10:182.

Irmler S, Schröder G, St-Pierre B, Crouch NP, Hotze M, Schmidt J, et al. Indole alkaloid biosynthesis in *Catharanthus roseus*: new enzyme activities and identification of cytochrome P450 CYP72A1 as secologanin synthase. Plant J 2000;24:797–804.

Jørgensen K, Rasmussen AV, Morant M, Nielsen AH, Bjarnholt N, Zagrobelny M, et al. Metabolon formation and metabolic channeling in the biosynthesis of plant natural products. Curr Opin Plant Biol 2005;8:280–91.

Kornblatt JA, Zhou JM, Ibrahim RK. Structure–activity relationships of wheat flavone O-methyltransferase: a homodimer of convenience. FEBS J 2008;275:2255–66.

Kutchan TM. A role for intra- and intercellular translocation in natural product biosynthesis. Curr Opin Plant Biol 2005;8:292–300.

Levac D, Murata J, Kim WS, De Luca V. Application of carborundum abrasion for investigating the leaf epidermis: molecular cloning of *Catharanthus roseus* 16-hydroxytabersonine-16-O-methyltransferase. Plant J 2008;53:225–36.

Liu CJ, Dixon RA. Elicitor-induced association of isoflavone *O*-methyltransferase with endomembranes prevents the formation and 7-*O*-methylation of daidzein during isoflavonoid phytoalexin biosynthesis. Plant Cell 2001;13:2643–58.

Mahroug S, Courdavault V, Thiersault M, St-Pierre B, Burlat V. Epidermis is a pivotal site of at least four secondary metabolic pathways in *Catharanthus roseus* aerial organs. Planta 2006;223:1191–200.

Murata J, De Luca V. Localization of tabersonine 16-hydroxylase and 16-OH tabersonine-16-*O*-methyltransferase to leaf epidermal cells defines them as a major site of precursor biosynthesis in the vindoline pathway in *Catharanthus roseus*. Plant J 2005;44:581–94.

Murata J, Roepke J, Gordon H, De Luca V. The leaf epidermome of *Catharanthus roseus* reveals its biochemical specialization. Plant Cell 2008;20:524–42.

Roepke J, Salim V, Wu M, Thamm AM, Murata J, Ploss K, et al. Vinca drug components accumulate exclusively in leaf exudates of Madagascar periwinkle. Proc Natl Acad Sci U S A 2010;107:15287–92.

Saslowsky DE, Warek U, Winkel BS. Nuclear localization of flavonoid enzymes in Arabidopsis. J Biol Chem 2005;280:23735–40.

Schröder G, Unterbusch E, Kaltenbach M, Schmidt J, Strack D, De Luca V, et al. Light-induced cytochrome P450-dependent enzyme in indole alkaloid biosynthesis: tabersonine 16-hydroxylase. FEBS Lett 1999;458:97–102.

Schuler MA, Werck-Reichhart D. Functional genomics of P450s. Annu Rev Plant Biol 2003;54:629–67.

St-Pierre B, De Luca V. A cytochrome P-450 monooxygenase catalyzes the first step in the conversion of tabersonine to vindoline in *Catharanthus roseus*. Plant Physiol 1995;109:131–9.

St-Pierre B, Laflamme P, Alarco AM, De Luca V. The terminal *O*-acetyltransferase involved in vindoline biosynthesis defines a new class of proteins responsible for coenzyme A-dependent acyl transfer. Plant J 1998;14:703–13.

St-Pierre B, Vazquez-Flota FA, De Luca V. Multicellular compartmentation of *Catharanthus roseus* alkaloid biosynthesis predicts intercellular translocation of a pathway intermediate. Plant Cell 1999;11:887–900.

Vazquez-Flota F, De Carolis E, Alarco AM, De Luca V. Molecular cloning and characterization of desacetoxyvindoline-4-hydroxylase, a 2-oxoglutarate dependent-dioxygenase involved in the biosynthesis of vindoline in *Catharanthus roseus* (L.) G. Don. Plant Mol Biol 1997;34:935–48.

Waadt R, Schmidt LK, Lohse M, Hashimoto K, Bock R, Kudla J. Multicolor bimolecular fluorescence complementation reveals simultaneous formation of alternative CBL/CIPK complexes in planta. Plant J 2008;56:505–16.

Wang R, Brattain MG. The maximal size of protein to diffuse through the nuclear pore is larger than 60 kDa. FEBS Lett 2007;581:3164–70.

Weis K. Regulating access to the genome: nucleocytoplasmic transport throughout the cell cycle. Cell 2003;112:441–51.

Westekemper P, Wieczorek U, Gueritte F, Langlois N, Langlois Y, Potier P, et al. Radioimmunoassay for the determination of the indole alkaloid vindoline in *Catharanthus*. Planta Med 1980;39:24–37.

Yu XH, Chen MH, Liu CJ. Nucleocytoplasmic-localized acyltransferases catalyze the malonylation of 7-O-glycosidic (iso)flavones in *Medicago truncatula*. Plant J 2008;55:382–96.